Electronic Supplementary Information

A highly thermal conductive electrode for lithium ion batteries

Bo Zhao, [a] Li Jiang, [a] Xiaoliang Zeng, [a] Kai Zhang, [b] Matthew M. F. Yuen, [b] Jian-Bin Xu, [c] Xian-Zhu Fu,[*,a] Rong Sun, [*,a] Ching-Ping Wong [c, d]

[a] Shenzhen Institutes of Advanced Technology, Chinese Academy of Sciences, Shenzhen, China.

[b] Department of Mechanical Engineering, The Hong Kong University of Science and Technology, Clear Water Bay, Kowloon, Hong Kong, China.

[c] Department of Electronics Engineering, The Chinese University of Hong Kong, Hong Kong, China.

[d] School of Materials Science and Engineering, Georgia Institute of Technology, Atlanta, GA 30332, United States.

[*] Corresponding author:

Xian-Zhu Fu, E-mail address: xz.fu@siat.ac.cn;

Rong Sun, E-mail address: rong.sun@siat.ac.cn.

Tel: +86-755-86392151; Fax: +86-755-86392299

1. The experimental setup of electrochemical exfoliation graphite rod

The experimental setup for electrochemical preparation of SnO_2 decorated graphene nanosheets (EGS) is illustrated in Fig. S1a. When a positive 10 V voltage is applied to a graphite anode electrode, bubbles are observed around the graphite rod electrode. Then the graphite rod begins to expand, quickly dissociates, spreads into the solution and the color of the aqueous electrolyte gradually changes from transparent to dark during the electrochemical exfoliation process. After 30 min exfoliation, the anode graphite rod becomes slim even disappear (Fig. S1b). The exfoliated graphitic material is collected by vacuum filtration and washed repeatedly with water to remove the residual electrolyte. Finally, the obtained powders were re-dispersed in DMF (Fig.S1c). The solution of EGS in DMF with a concentration of about 2.0 mg mL^{-1} is very stable, which could be keep dispersion for several weeks without agglomeration. The exfoliation process is readily scaled up due to the easy-operating process, which by only using a several centimeters long graphite electrode, hundreds milligram of EGS powders could be obtained within one hour (Fig. S1d).

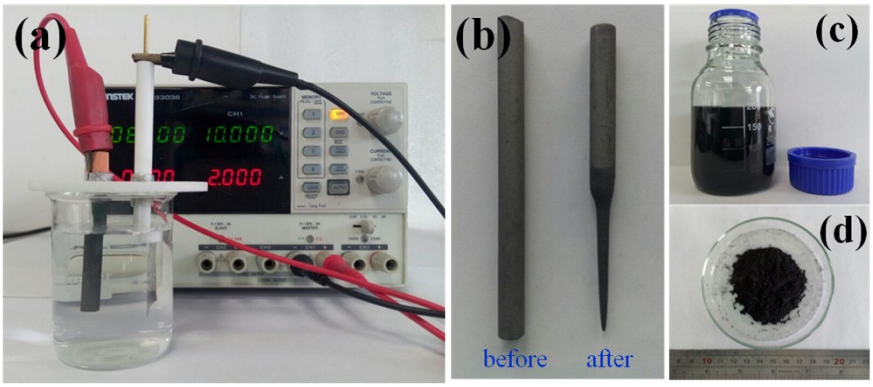

Fig. S1. Photograph of (a) electrochemical preparation of SnO_2 decorated graphene nanosheets setup, (b) graphite rod before and after exfoliation, (c) dispersed graphene sheets (~2.0 mg mL^{-1}) in DMF, (d) the product of graphene powder.

2. The mechanism of electrochemical exfoliation

Fig. S2 demonstrates the possible preparation mechanism of EGS by simultaneous electrolytic method: Firstly, applying bias voltage results in water splitting at the cathode, producing hydroxyl (•OH) and oxygen radicals (•O), hydroxyl ions (OH^-) that act as a strong nucleophile in the electrolyte. The nucleophilic attacks graphite by OH^- ions initially occurs at the edge sites and grain boundaries (the first step). Secondly, defective sites at the edges or grain boundaries of graphite rod begin to oxide, which leads to depolarization, expansion and open up of the graphite layers. It is beneficial to the intercalation of stannate ions (SnO_3^{2-}) within the graphitic layers (the second step). During this stage, water molecules can co-intercalate into the graphite layers with the SnO_3^{2-} anions. Thirdly, the SnO_3^{2-} anions are reduced to SnO_2 nanoparticles on the graphite nanosheets and self-oxidation of water produces gaseous O_2. In addition, these gaseous species can exert large forces to separate weakly bonded graphite layers from one another to form graphene nanosheets.[1-3]

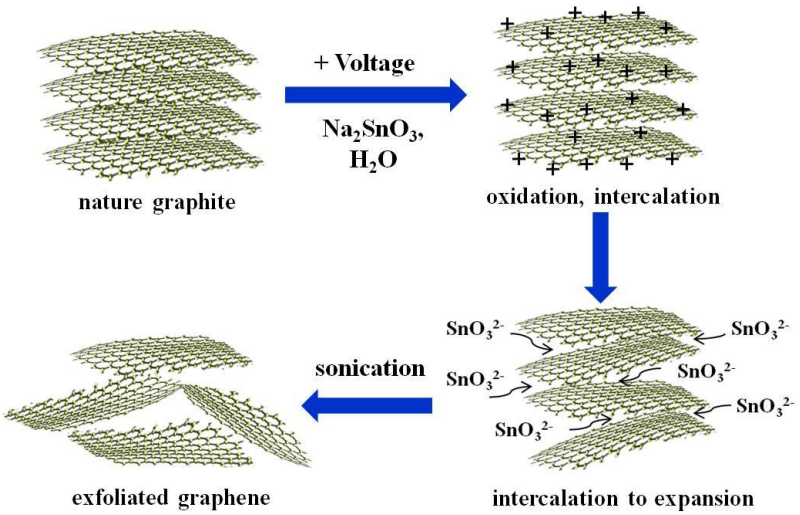

Fig. S2. schematic illustration of the proposed mechanism of electrochemical exfoliation.

3. The morphology changes of graphite rod during the electrochemical process

A constant bias voltage +10 V is also applied to graphite electrodes for different time periods 0 s~30 min and the morphologies of exfoliated graphite rod are shown in Fig. S3. The surface of graphite rod is relative smooth and flat before exfoliation (Fig.S3a). After applying voltage for 10 s, the edge of the graphite rod expands and the cracks in the graphite layers increase (Fig. S3b). When the time increases to 30 s, the boundaries are opened up, a large amount of fissures between the graphite flakes are observed, suggesting the successful exfoliation of graphite rod (Fig. S3c). When extend to 1min, the edge of the graphite rod exfoliates further, the exfoliated sheets begin to crimp. It indicates that the exfoliated graphene sheet is too thin to keep flat due to the high surface energy.[4] Due to the abundant visible gas bubbles evolution causing expansion and swelling of the graphite layers, a network of ripples on the surface of the graphite is clearly identified in the SEM images (Fig. S3d). Simultaneously, the solution becomes more and more turbid for lots of graphene nanosheets diffuse into the electrolyte (Fig. S3e). When the graphite rod is exfoliated completely, most of the obtained graphene nanosheets are wrinkled and interweave each other, suggesting the excellent exfoliation effects (Fig. S3f). These observations strongly support that the edge of graphite rod begins to open up first, then anion intercalation and gas entrance, facilitate to obtain exfoliated graphene nanosheets in the electrochemical process.[5-6]

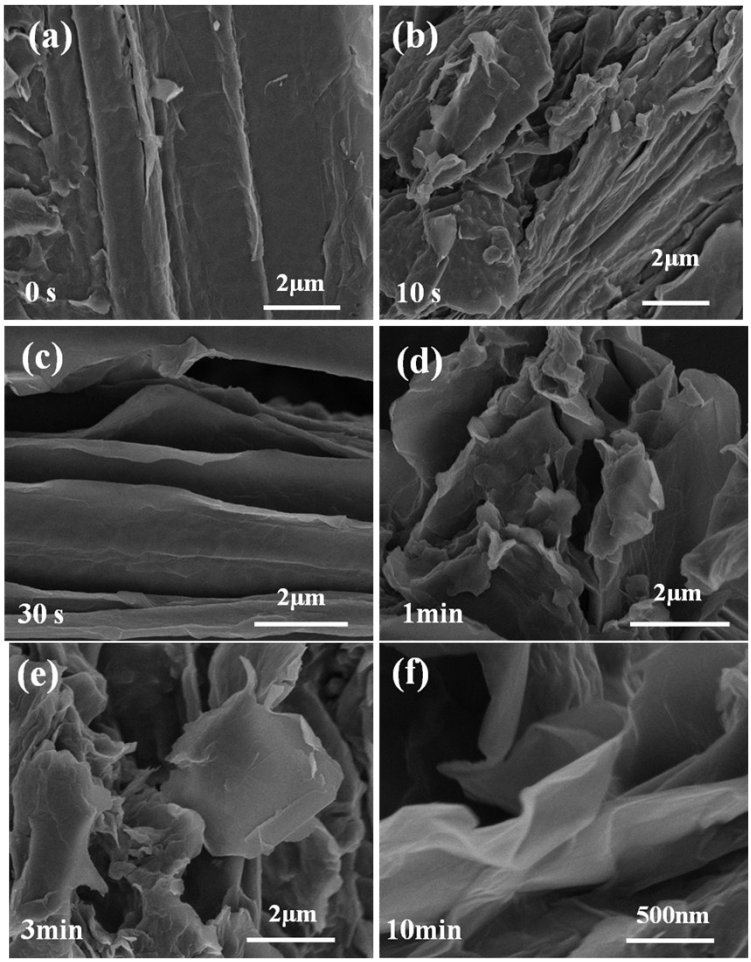

Fig. S3. SEM images of graphite rod during the electrochemical process after applying a bias voltage of +10 V for 0, 10, 30s, 1min, 3 min and 10 min in aqueous Na_2SnO_3 electrolyte solution, respectively.

4. The morphology of exfoliated graphene in H_2SO_4 electrolyte

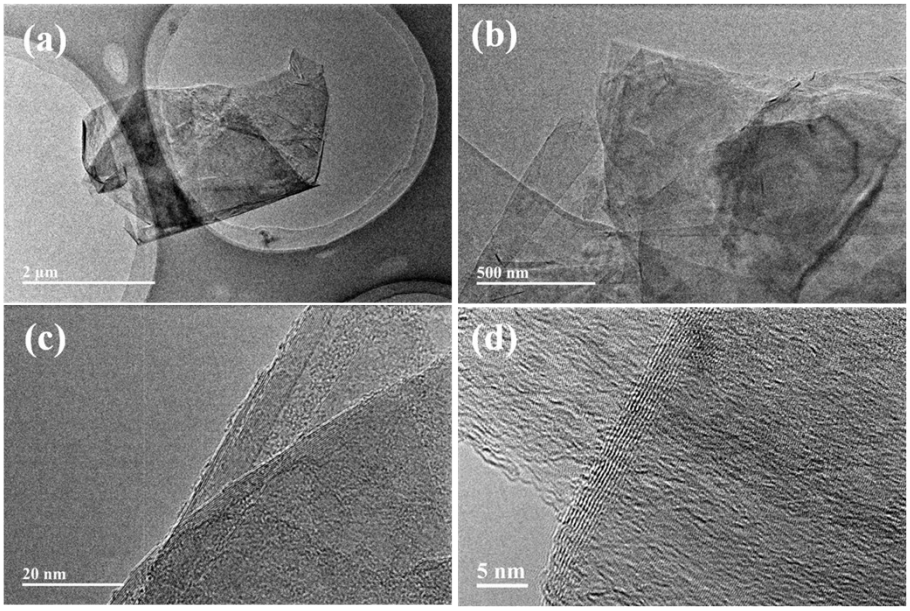

Fig. S4. The different magnifications TEM images of exfoliated graphene (EG) in 0.1M H_2SO_4 solution at 10V applied voltage.

5. The principle of laser flash method for measuring in-plane thermal diffusivity and the calculation method of thermal conductivity:

The thermal diffusivity of the film samples were measured by a NETZSCH LFA 467 light flash system. The in-plane diffusivity was measured by using a special sample holder, which sends the thermal energy along the sample (Fig. S5). A mask with a hole makes the light energy input on the bottom of the sample and heat will flow through the thickness of the sample and spread out in the plane. Another mask with embedded annulus is placed on the sample to allow heat radiation to be collected by the IR detector. In this case, the large anisotropy of the film sample in heat conduction would affect the in-plane measurement, i.e. the time for the heat to reach the slit in the mask will depend on both the radial diffusion time and the axial diffusion time. Thus, the "anisotropic + heat loss" model was used to calculate the in-plane diffusivity. The through-plane diffusivity of the sample was measured firstly and input to the in-plane analysis and used in the axial part of the heat flow calculation. Then an iterative scheme is used to separate the axial and radial diffusivities. To calculate the thermal conductivity of the film, the apparent density (ρ, $g \cdot cm^{-3}$) of the film was measured by dividing the mass over the volume $\rho = m/V$. The 25.4 mm diameter disk film was punched out for the in-plane thermal diffusivity measurement. The thickness (h) of these films was measured with SEM. The volume (V) was obtained according to the formulas $V = \pi \times 12.7 \times 12.7 \times h = 506.45 \times h$. and the value of specific heat capacity (Cp, $J \cdot g^{-1}K^{-1}$) was measured by DSC (NETZSCH, DSC200F3). The thermal conductivity (λ, $W \cdot m^{-1}K^{-1}$) was calculated according to the equation: $\lambda = \alpha \times \rho \times Cp$.

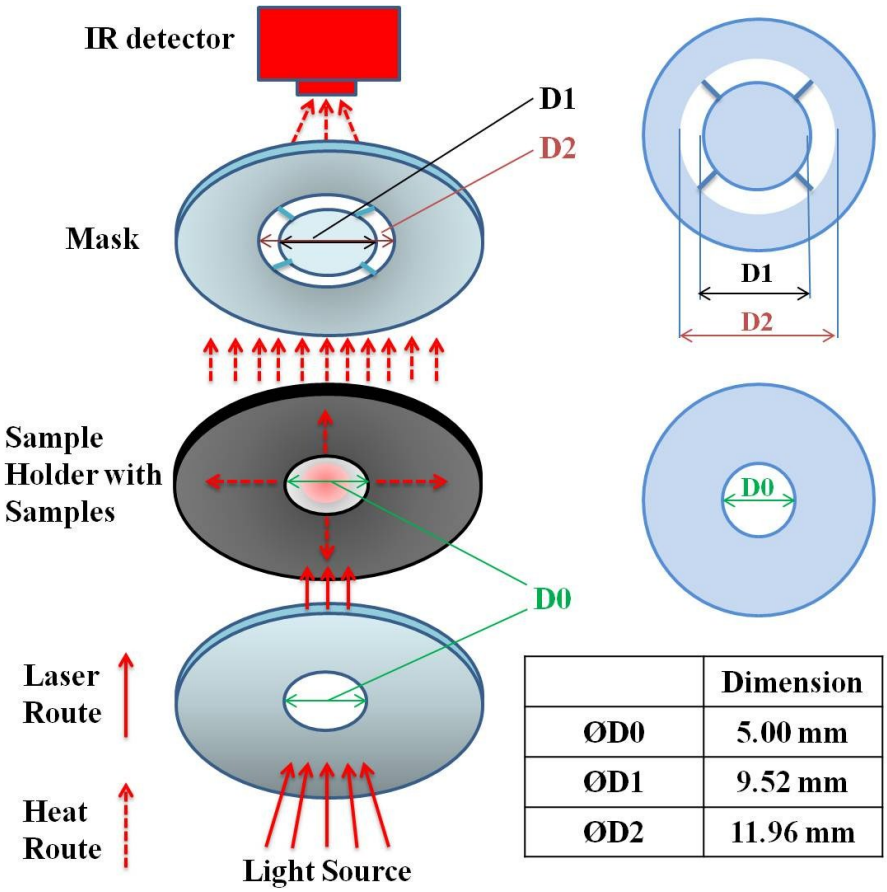

	Dimension
ØD0	5.00 mm
ØD1	9.52 mm
ØD2	11.96 mm

Fig. S5. Schematic illustration diagram of the laser flash method for measuring in-plane thermal diffusivity.

6. The first three cycles CV curves of EG, SnO_2 and EGS

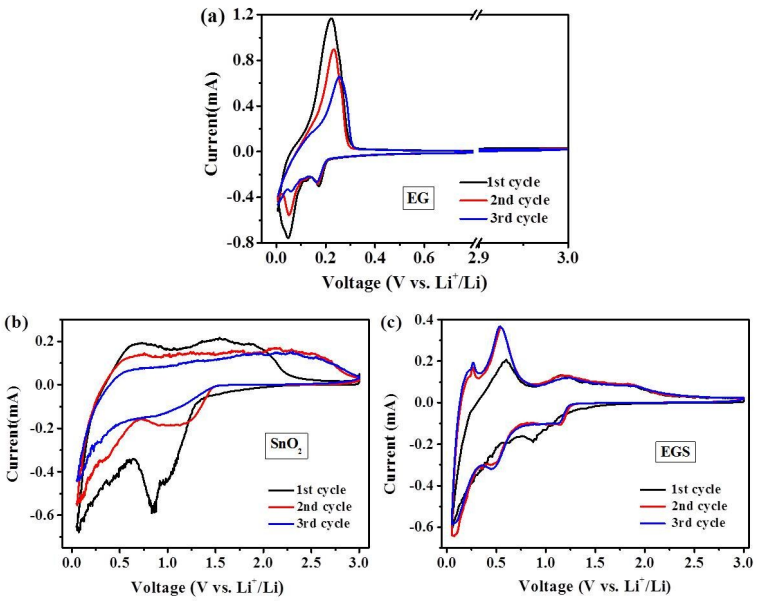

Fig. S6. The CV curves of the first, second and third cycles of (a) EG, (b) SnO_2 nanoparticles and (c) EGS electrodes at a scan rate of 0.1 mV s^{-1} over the voltage range of 0.01~3.0 V.

References

S1. C. Y. Su, A. Y. Lu, Y. Xu, F. R. CHen, A. N. Khlobystov, L. J. Li*, ACS Nano*, 2011**, 5**, 2332-2339.

S2. K. Kakaei, *Carbon*, 2013**, 51**, 195-201.

S3. K. Parvez, Z. S. Wu, R. Li, X. Liu, R. Graf, X. L. Feng, K. Muellen, *J. Am. Chem. Soc*, 2014**, 136**, 6083-6091.

S4. A. M. Abdelkader, I. A. Kinloch, R. A. W. Dryfe, *ACS Appl. Mater. Inter*, 2014**, 6**, 1632-1639.

S5. S. Yang, S. Bruller, Z. S. Wu, Z. Liu, K. Parvez, R. Dong, F. Richard, P. Samori, X. L. Feng, K. Mullen, *J. Am. Chem. Soc*, 2015**, 137**, 13927-32.

S6. J. Liu, M. Notarianni, G. Will, V. T. Tiong, H. Wang, N. Motta, *Langmuir*, 2013**, 29**, 13307-13314.